Characterization of photophysical and base-mimicking properties of a novel fluorescent adenine analogue in DNA

Anke Dierckx[1], Peter Dinér[2], Afaf H. El-Sagheer[3,4], Joshi Dhruval Kumar[1], Tom Brown[3], Morten Grøtli[2] and L. Marcus Wilhelmsson[1,*]

[1]Department of Chemical and Biological Engineering/Physical Chemistry, Chalmers University of Technology, [2]Department of Chemistry, Medicinal Chemistry, University of Gothenburg, S-41296 Gothenburg, Sweden, [3]School of Chemistry, University of Southampton, Highfield, Southampton SO17 1BJ, UK and [4]Department of Science and Mathematics, Chemistry Branch, Faculty of Petroleum and Mining Engineering, Suez Canal University, Suez 43721, Egypt

ABSTRACT

To increase the diversity of fluorescent base analogues with improved properties, we here present the straightforward click-chemistry-based synthesis of a novel fluorescent adenine-analogue triazole adenine (A^T) and its photophysical characterization inside DNA. A^T shows promising properties compared to the widely used adenine analogue 2-aminopurine. Quantum yields reach >20% and >5% in single- and double-stranded DNA, respectively, and show dependence on neighbouring bases. Moreover, A^T shows only a minor destabilization of DNA duplexes, comparable to 2-aminopurine, and circular dichroism investigations suggest that A^T only causes minimal structural perturbations to normal B-DNA. Furthermore, we find that A^T shows favourable base-pairing properties with thymine and more surprisingly also with normal adenine. In conclusion, A^T shows strong potential as a new fluorescent adenine analogue for monitoring changes within its microenvironment in DNA.

INTRODUCTION

Fluorescence is a very powerful and commonly used technique for the study of macromolecules, such as DNA, RNA and proteins (1). The virtually non-fluorescent nature of the regular nucleic acid bases makes artificial fluorophores such as fluorescent base analogues important and excellent tools in investigations of DNA or RNA systems. Fluorescent base analogues are significantly emissive molecules which are similar in shape to natural nucleobases and are able to form one or more hydrogen bonds to a natural nucleobase in the complementary strand. This means that these artificial bases do not radically alter the structure of DNA, and therefore they have major advantages compared to other dyes which are covalently tethered to the DNA outside the base-stack (e.g. Cy-dyes, fluorescein, Alexa dyes or rhodamines). Importantly, fluorescent base analogues allow experiments to be performed while preserving the native structure of DNA by avoiding bulky external probes. Furthermore, they are located rigidly in the DNA base-stack, in contrast to the covalently attached dyes, and this restricted movement results in a more predictable orientation which can therefore yield more reliable fluorescence resonance energy transfer (FRET) data and fluorescence anisotropy data. These probes have therefore become increasingly popular over the past decade for studying interactions between DNA/RNA and other molecules and to explore nucleic acid structure.

Over the past years various classes of base analogues have been developed, each with specific properties. With exception of the tricyclic cytosine family described in more detail below, virtually all these classes show significant sensitivity to their microenvironment. The pyrimidine analogues designed by Tor and co-workers (2–4), pyrrolo-dC (5), the blue fluorescent triazole deoxycytidine analogues (6) and the base discriminating fluorescent bases (BDF) designed by Saito and co-workers (7–11) are just a few examples of this expanding class of molecules. Furthermore, the pteridine analogues of guanine (3-MI and 6-MI) (12–15) and adenine (6-MAP and DMAP) (16) have also been studied thoroughly. Other interesting purine analogues are the adenine analogues A-3CPh and

A-4CPh that show an increased emission inside RNA (17,18) and the 7-deazapurines (19,20). Recently, our group has developed and extensively characterized a class of tricyclic cytosine analogues, tC, tC^o and tC$_{nitro}$. Surprisingly, neither tC nor tC^o show sensitivity to their environment in duplex DNA. Lately, we also presented tC^o and the non-emissive tC$_{nitro}$ as the first nucleobase FRET-pair, yielding accurate distance and orientation information in DNA (21–23). [for recent reviews on fluorescent (nucleic acid base) analogues, see references (24), (25) and (1)].

One of the most widely used fluorescent base analogues is the adenine analogue 2-aminopurine, which shows a quantum yield of 0.68 in water. However, this decreases dramatically in both single- (0.007–0.02) and double-stranded DNA (0.0007–0.01) (26). Moreover, a destabilization of the duplex of 10°C has been determined using melting studies (27). Furthermore, 2-aminopurine is capable of forming base pairs with both thymine and cytosine and is, thus, not selective (28,29). Nonetheless, it has found use in countless studies as discussed further below.

Fluorescent nucleic acid base analogues have found many applications over the years, of which only a few will be highlighted here [for a broader overview see (1,24,30,31)]. The future perspective of personalized medicine is to allow treatment based on individual genetic data. With this objective in mind, the detection of single nucleotide polymorphisms (SNP) has gained increasing attention and fluorescent base analogues, such as the class of BDF analogues developed by Saito and co-workers have been designed for this purpose. The principle is based on these analogues showing a distinct difference in emissive signal depending on the opposite base (7–10). Furthermore, many analogues are recognized as substrates by DNA/RNA polymerases and have consequently been used in studies concerning the enzyme mechanism, kinetics, substrate specificity and fidelity (5,32–38). 2-Aminopurine has been used in numerous studies on T4 DNA polymerase and Klenow fragment binding to primer-template DNA as well as T7 RNA polymerase interaction with the DNA promotor (39–44). Also, in studies on the mechanism of other proteins and their binding to RNA or DNA, fluorescent base analogues have been proven to be highly useful. An excellent example of such an application for DNA is the role of 3-MI in an investigation of the dissociation of the multimeric form of the HIV-1 integrase complex upon DNA binding (45). In the RNA-context, protein binding studies have also been performed using fluorescent base analogues, for example, 2-aminopurine has been utilized in studies of adenosine deaminases (ADARs) which play a role in RNA editing of eukaryotic pre-mRNA (46,47). Finally, fluorescent base analogues have recently entered the area of DNA nanotechnology, exemplified by the use of tC^o in monitoring the local stability of self-assembling DNA hexagons (48).

Here we report the synthesis and photophysical characterization of a new fluorescent adenine analogue in DNA, 8-(1-pentyl-1H-1,2,3-triazole-4-yl)-2′-deoxyadenosine (A^T) (Figure 1), which shows promising features
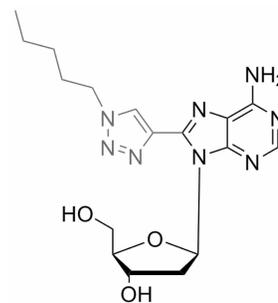

Figure 1. Structure of 8-(1-pentyl-1H-1,2,3-triazole-4-yl)-2′-deoxyadenosine, A^T, in which the triazole ring with *n*-pentyl, added to the normal adenine structure, is shown in grey.

compared to other fluorescent adenine analogues such as the commercially available 2-aminopurine. In a previous investigation, several adenosine derivatives of A^T were studied and shown to exhibit a very high-quantum yield in THF and red-shifted absorption relative to the DNA absorption band. One of the compounds, having an isopentyl substituent in the triazole ring, showed a very high-quantum yield in both THF (0.62) and water (>0.50) (49). In this work, we characterize the 2′-deoxyadenosine form of A^T both in methanol and water. In addition, we have incorporated it into 10 different 10-mer oligonucleotides with various base-stacking environments in order to perform a photophysical and structural characterization of A^T in DNA. We find that A^T causes only minor perturbations to natural B-DNA. Furthermore, quantum yields for A^T incorporated into single- and double-stranded DNA reach maximum values that far exceed corresponding values for 2-aminopurine. Moreover, we have investigated the base-pairing specificity of A^T with all four natural DNA-bases. To our surprise, we find that A^T forms equally stable base pairs with thymine and adenine. In conclusion, A^T is a very promising new fluorescent base analogue, showing high sensitivity to its microenvironment.

MATERIALS AND METHODS

The synthesis of 8-(1-pentyl-1H-1,2,3-triazole-4-yl)-2′-deoxyadenosine and of the triazolyl 2′-deoxyadenosine phosphoramidite monomer (see Scheme 1 in 'Results' section) as well as its incorporation into oligonucleotides and purification of the oligonucleotide strands are described in the Supplementary Data S1.

Sample preparation

All samples used in this work, unless stated otherwise, were prepared in a sodium phosphate buffer, pH 7.5 with a total salt concentration of 500 mM. The oligonucleotide concentration was determined by measuring the absorption at 260 nm. The extinction coefficients of the modified oligonucleotide single strands (sequences listed in Table 1) were calculated by summation of the extinction coefficients of the natural oligonucleotides and of the A^T-monomer. This sum was multiplied by 0.9
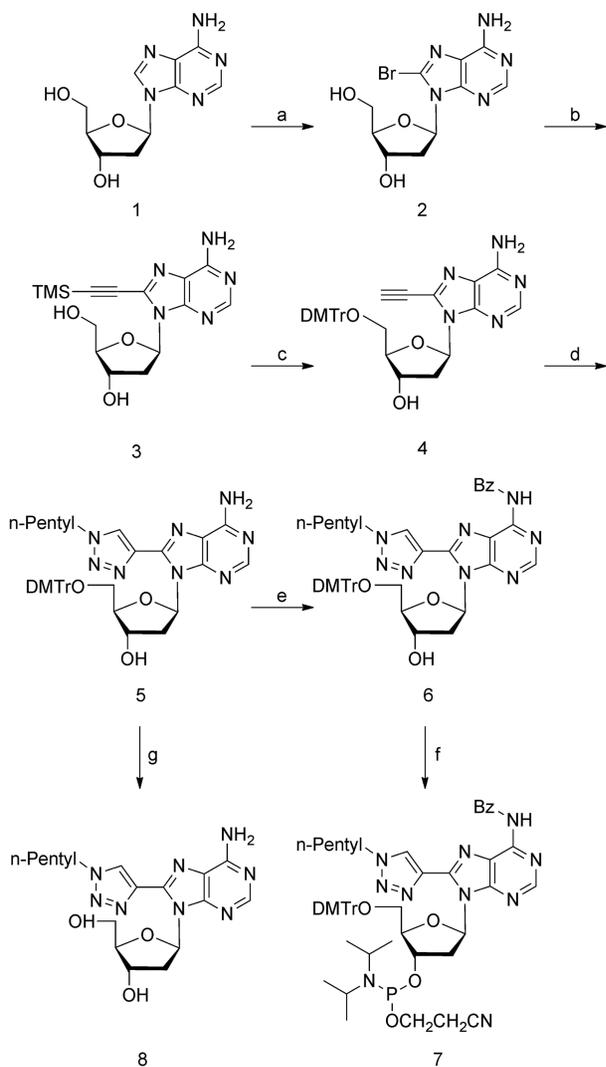
Scheme 1. (a) Br$_2$/NaOAc-buffer, r.t., overnight, 81%. (b) Pd(PPh$_3$)$_4$ (4 mol%), CuI (8 mol%), TMS-acetylene, Amberlite IRA-67, THF, 40°C, 2 h, 91%. (c) (i) DMTrCl, pyridine, overnight, r.t.; (ii) NH$_3$ (25% aq.), 2 h 65%. (d) (i) Pentylbromide, NaN$_3$, water, 140°C, 1 h; (ii) CuI, ethyl acetate, 14 h, r.t., 76%. (e) (i) TMSCl, pyridine, 2 h; (ii) BzCl, 3 h; (iii) Water, 15 min then NH$_3$ (aq.), 30 min, 68%. (f) DIPEA (0.11 ml, 0.64 mmol), 2-Cyanoethyl-*N,N*-diisopropylchlorophosphoramidite, DCM, 1 h, 91%. (g) Acetic acid, 30 min, 34%.

to correct for base-stacking interactions. The extinction coefficient of the highly soluble A^T was determined by dissolving 1.4 mg of compound in 50 ml of methanol. An absorption shift of 4 nm was observed compared to A^T in Milli-Q water. The extinction coefficient of A^T in water was therefore calculated using the absorption value at 264 nm in methanol (9400 M^{-1}cm^{-1}). The extinction coefficients that were used for the different bases at 260 nm were $\varepsilon_T = 9300$ M^{-1}cm^{-1}, $\varepsilon_C = 7400$ M^{-1}cm^{-1}, $\varepsilon_G = 11\,800$ M^{-1}cm^{-1}, $\varepsilon_A = 15\,300$ M^{-1}cm^{-1} and $\varepsilon_{AT} = 9400$ M^{-1}cm^{-1}. Using these values, the following extinction coefficients were obtained for the modified oligonucleotides: $\varepsilon_{GA} = 95\,900$ M^{-1}cm^{-1}, $\varepsilon_{CT} = 86\,500$ M^{-1}cm^{-1}, $\varepsilon_{GC} = 88\,800$ M^{-1}cm^{-1}, $\varepsilon_{CA} = 91\,900$ M^{-1}cm^{-1}, $\varepsilon_{GG} = 92\,700$ M^{-1}cm^{-1}, $\varepsilon_{CC} = 84\,800$ M^{-1}cm^{-1}, $\varepsilon_{TA} = 93\,600$ M^{-1}cm^{-1}, $\varepsilon_{AA} = 99\,000$ M^{-1}cm^{-1}, $\varepsilon_{AC} = 91\,900$

Table 1. DNA melting temperatures of the 10 A^T-modified DNA-duplexes ($T_m{}^{AT}$), the corresponding unmodified duplexes ($T_m{}^A$) and the difference in melting temperature between them (ΔT_m)

DNA sequence[a]	Neighbouring bases = name of oligomer[b]	$T_m{}^{AT}$ (°C)[c]	$T_m{}^A$ (°C)[c]	ΔT_m (°C)
5′-d(CGCACA**T**ATCG)-3′	*CA*	43	52	−9
5′-d(CGCAGA**T**GTCG)-3′	**GG**	45	54	−9
5′-d(CGCAAA**T**ATCG)-3′	**AA**	41	50	−9
5′-d(CGCATA**T**ATCG)-3′	*TA*	39	47	−8
5′-d(CGCATA**T**GTCG)-3′	*TG*	42	50	−8
5′-d(CGCAGA**T**ATCG)-3′	**GA**	43	50	−7
5′-d(CGCACA**T**TTCG)-3′	*CT*	45	52	−7
5′-d(CGCAAA**T**CTCG)-3′	**AC**	46	53	−7
5′-d(CGCACA**T**CTCG)-3′	*CC*	49	56	−7
5′-d(CGCAGA**T**CTCG)-3′	**GC**	49	54	−5

[a]For the unmodified strands A^T is replaced by A.
[b]Purines neighbouring A^T are shown in bold and pyrimidines are shown in italic.
[c]Samples were prepared in phosphate buffer (500 mM Na$^+$, pH 7.5) at a duplex concentration of 2.5 μM.

M^{-1}cm^{-1} and $\varepsilon_{TG} = 90\,400$ M^{-1}cm^{-1}. Extinction coefficients of the unmodified oligonucleotides were calculated in the same way.

UV melting experiments

Equal volumes of 5 μM solutions of single-stranded oligonucleotides in buffer were mixed at room temperature. In order to achieve a correct and complete hybridization the samples were heated to 85°C, followed by cooling to 5°C at the rate of 1°C/min. Next, data were recorded during heating of the samples to 85°C, followed by cooling to 5°C at a rate of 0.5°C/min. The temperature was kept at 85°C for 5 min between heating and cooling. For unmodified duplexes a temperature range of 15°C to 92°C was used for recording those data. The melting curves were obtained on a Varian Cary 4000 spectrophotometer with a programmable multi-cell temperature block using an absorption wavelength of 260 nm. Melting temperatures presented in this article are averages of the temperature values at the maximum of the first derivative and at half maximum of the melting curves and were measured at least twice.

Circular dichroism

Circular dichroism (CD) spectra were recorded on a Chirascan CD spectrophotometer at 25°C. Spectra of all samples were recorded between 200 and 350 nm and corrected for background contributions. Spectra of solutions containing 2.5 μM DNA duplexes, prepared as described above, were recorded and data were averaged over at least five measurements at a scan rate of 2 nm/s.

Steady-state fluorescence measurements

Quantum yields (Φ_f) of the A^T-monomer and the different A^T-modified oligonucleotides were determined relative to the quantum yield of quinine sulphate ($\Phi_f = 0.55$) in 0.5 M H$_2$SO$_4$ at 25°C (50). Samples containing duplex DNA were prepared as described above. The monomer or samples containing single-stranded oligonucleotides were

set to an absorption of ∼0.03 at the excitation wavelength. Spectra were recorded on a SPEX fluorolog 3 spectrofluorimeter (JY Horiba). For the duplexes and single-stranded oligonucleotides an excitation wavelength of 300 nm was used and emission spectra were recorded between 305 and 550 nm. The monomer was excited at 282 nm and the emission was monitored between 290 and 700 nm. For the reference, quinine sulphate, emission was recorded between 305 and 700 nm.

Steady-state excitation anisotropy spectra were recorded on a SPEX fluorolog 3 spectrofluorimeter (JY Horiba) using Glan polarizers and emission was measured at 355 nm using excitation wavelengths from 280 to 340 nm. The polarized excitation spectra of the A^T-monomer were recorded between 240 and 350 nm in a H_2O:ethylene glycol (1:2 mixture) glass at $-100°C$, monitoring the emission at 352 nm. The fluorescence anisotropy was calculated as:

$$r = \frac{I_{VV} - GI_{VH}}{I_{VV} + 2GI_{VH}}$$

where the instrumental correction factor

$$G = \frac{I_{HV}}{I_{HH}}$$

and I_{XY} is the excitation spectrum for which the subscripts X and Y denote polarization directions of the excitation and emission light, respectively, and H and V refers to horizontal and vertical, respectively. For an immobile fluorophore, such as A^T in H_2O/ethylene glycol glass, the fundamental anisotropy (r_{0i}) for a certain transition (i) is related to the angle between the absorbing and the emitting transition moments as follows:

$$r_{0i} = \frac{1}{5}\left(3\cos^2\alpha_i - 1\right).$$

Time-resolved fluorescence measurements

Fluorescence lifetimes were measured using time-correlated single-photon counting. The excitation pulse was generated with a Tsunami Ti:sapphire laser (Spectra-physics) that was pumped by a Millenia Pro X laser (Spectra-Physics). The Tsunami output was tuned to 900 nm and frequency-tripled to 300 nm. Samples were excited with a repetition rate of 80 MHz, a 1-2 ps pulse width, IRF 70 ps (FWHM) and a time-window of 10 ns. However, for the A^T monomer and the single stranded samples **AA** and **G**C (Table 1) the frequency was reduced to 4 MHz by a pulse picker (Spectra physics, Model 3985) and a time window of 20 ns was used. The emission was monitored at 355 nm and photons were collected by a microchannel-plate photomultiplier tube (MCP-PMT R3809U-50; Hamamatsu). These counts were fed into a multichannel analyzer with 4096 channels (Lifespec, Edinburgh Analytical Instruments), where a minimum of 10 000 counts were recorded in the top channel. The intensity data were convoluted with the instrument response function and fitted to one-, two- or three-exponential expressions with the program Fluofit Pro v.4 (PicoQuant GmbH).

Computation of the internal wobble of A^T in DNA

Duplex samples of strands **AA** and *T*A (Table 1) were prepared as described above in phosphate buffer (500 mM Na^+, pH 7.5) containing 65% (w/v) ($\eta/\eta_{water} \approx$ 20) and 77.2% (w/v) sucrose ($\eta/\eta_{water} \approx$ 58). An excess of 12% of the unmodified strand was used. Samples were annealed by heating to 75°C for 20 min, followed by slow cooling to room temperature. Steady-state excitation anisotropy measurements were performed as described above for which spectra were averaged over 22 repeats and were corrected for background contributions. Internal dye motion was computed using an in-house designed Matlab program (S. Preus, personal communication) based on calculations carried out by Barkley and Zimm (51).

RESULTS

Synthesis of A^T phosphoramidite monomer

Starting from commercially available 2′-deoxyadenosine **1**, 8-bromoadenosine **2** was easily obtained using bromine in a sodium acetate buffer (Scheme 1) as previously described (52). The TMS-protected alkyne **3** was installed in the 8-position in good yield (91%) via a standard Sonogashira coupling protocol (53). The 5′-hydroxy group was protected using 4,4′-dimethoxytrityl chloride in dry pyridine, followed by an *in situ* deprotection of the TMS-group using aqueous ammonia (25%) yielding compound **4** in 65%. In the next step, the pentyl azide was generated *in situ* through the reaction between pentyl bromide and sodium azide, followed by the addition of compound **4** and copper iodide, yielding the cycloaddition product **5** in 76% yield. A small sample of compound **5** was treated with acetic acid to generate sufficient amount of **8** for measuring its fluorescence quantum yield and anisotropy. The exocyclic amino group of compound **5** was protected with a benzoyl group. In the last step, compound **7** was prepared using DIPEA and 2-cyanoethyl-*N*,*N*-diisopropylchlorophosphoramidite in dichloromethane (91%).

Spectroscopic characterization of the A^T monomer

The absorption and emission spectra of A^T, where the triazole-modified A-nucleobase constitutes the chromophoric/fluorophoric unit of the nucleoside, in Milli-Q water are shown in Figure 2. Their shapes are virtually identical to the corresponding spectra recorded for A^T in methanol (data not shown). In water, the lowest energy absorption band is centred at 282 nm with an extinction coefficient of 16 500 $M^{-1}cm^{-1}$ and the emission maximum is located at 353 nm. The absorption spectrum recorded for A^T in methanol shows a redshift of 4 nm compared to in water whereas a blueshift of 7 nm was observed for the corresponding emission spectrum of A^T. Moreover, A^T shows a very high quantum yield both in water (0.61) and in methanol (0.49). Furthermore, a lifetime of 1.8 ns
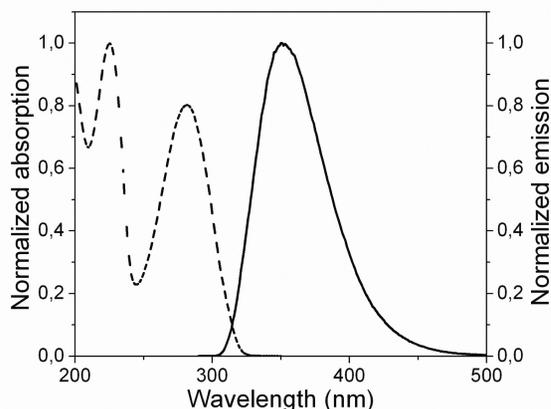
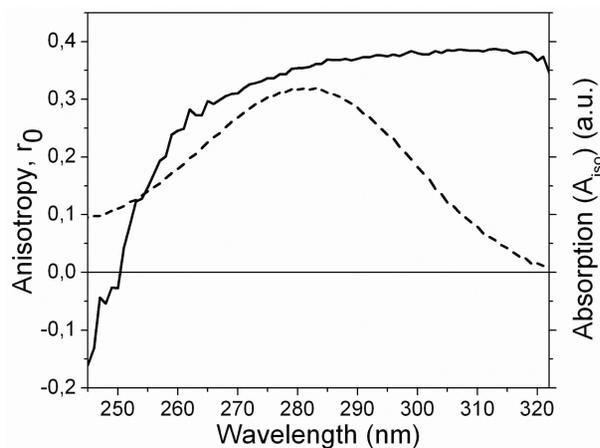**Figure 2.** Absorption (dashed line) and emission (solid line) spectrum of the A^T monomer in water.

Figure 3. Excitation anisotropy spectrum (r_0, solid line) of the A^T nucleoside in a H_2O/ethylene glycol glass (1:2 mixture) at $-100°C$. The isotropic absorption (A_{iso}, dashed line) is shown as a comparison and was measured in Milli-Q water.

was recorded for the A^T monomer in water. A small residual could be observed, which is most probably a result of small deviations in the instrument response function.

The fundamental fluorescence anisotropy of A^T (r_0, Figure 3) was measured in a H_2O/ethylene glycol glass (1:2 mixture). A constant value of $r_0 = 0.38$ can be observed between 280 and 320 nm, which approaches the theoretical maximum value of 0.4 and suggests that the emission and absorption transition moments are virtually parallel in this region. The constant r_0 value in this region also indicates a single transition dipole moment in this absorption band.

Structure and stability of DNA duplexes containing A^T

UV duplex melting experiments. The 10 modified and normal single-stranded DNA sequences that were used in this study are listed in Table 1. To examine the influence of various bases surrounding the modified adenine A^T, the neighbouring positions are varied in these 10 sequences. Sequences were designed in order to evaluate
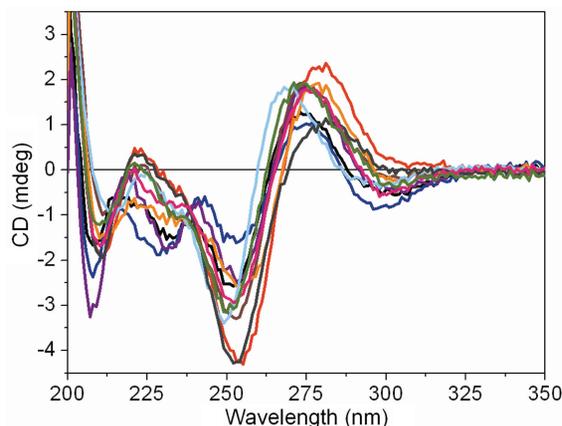

Figure 4. CD spectra of all 10 DNA duplexes containing the A^T analogue. Duplexes are denoted by the bases neighbouring A^T and consist of the modified strands **GA** (black), *CT* (red), **G**C (dark blue), **C**A (brown), **GG** (purple), *CC* (orange), *TA* (light blue), **AA** (grey), **A**C (pink) and *TG* (green) hybridized to the complementary natural DNA strand. Spectra were recorded in phosphate buffer (500 mM Na^+, pH 7.5) at 25°C at a duplex concentration of 2.5 μM.

combinations of purines and pyrimidines and their proximity both 3′ and 5′ to A^T. The melting temperatures of unmodified and modified duplexes prepared by mixing with their unmodified complementary DNA strands are presented in Table 1. Comparison between the melting temperatures of the modified and the corresponding unmodified duplexes shows an average drop in melting temperature of 8°C, and thus a destabilization of double stranded DNA upon incorporation of A^T. Further analysis of the changes in T_m suggests that sequences with purines 3′ of A^T have the largest destabilizing effect whereas pyrimidines at the 3′-side of A^T generally have a smaller effect.

Circular dichroism (CD). The CD spectra that were recorded for the duplexes, consisting of a modified strand containing one A^T (Table 1) and its unmodified complementary sequence are presented in Figure 4. Analysis of the spectra between 200 and 300 nm shows a high resemblance to the CD signature of a natural B-DNA-helix, which is characterized by a positive band at 275 nm, a negative band at 240 nm, a band which is less negative or positive at 220 nm and a narrow negative band in the region between 220 and 190 nm, preceded by a large positive peak at 180–190 nm. Some modified duplexes show an almost identical CD-spectrum to their natural DNA (*CT*, **C**A, *TG*, *CC* and **AA**) (Supplementary Data S2), whereas others show more distinct differences between the corresponding spectra (strands **GA**, **G**C, **GG**, *TA* and **A**C) (Supplementary Data S2). Sequences **GA**, **G**C and **GG**, having a guanine flanking A^T at the 5′-side, show the most perturbed CD signals. As an illustration of this variation, one of the latter spectra (**GG**) is shown in Figure 5 and compared to the CD spectrum of the corresponding unmodified helix and to the absorption difference between the modified and natural duplex of this sequence. The resulting differential absorption band correlates well to the regions (∼210, 230 and 295 nm) where

the CD-spectra of natural and modified duplexes differ most significantly (Figure 5).

Base pairing specificity. To investigate the ability of A^T to form base pairs with bases other than thymine, we chose three of the modified duplexes and replaced the base opposite A^T by a guanine, cytosine and adenine, respectively (Table 2). These three sequence contexts were chosen so that the influence of neighbouring bases could also be explored: A^T is surrounded either by (i) two purines, (ii) two pyrimidines or (iii) a purine and a pyrimidine. The melting temperatures and the quantum yields that were obtained for these mismatched duplexes are listed in Table 2. For comparison, the data recorded for the modified matched duplexes are also shown. The neighbouring bases did not significantly influence the depression in melting temperature caused by the mismatches.
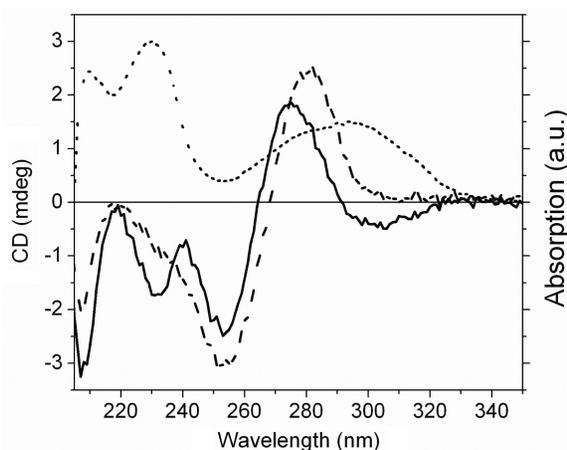

Figure 5. CD spectra of the modified **GG**-duplex (solid line) and of the corresponding natural duplex (dashed line). The difference in absorption spectra of A^T and A (dotted line) was obtained by subtracting the absorption spectra of equimolar solutions of the natural **GG**-duplex from the modified **GG**-duplex. Spectra were recorded in phosphate buffer (500 mM Na$^+$, pH 7.5) at 25°C at a duplex concentration of 2.5 μM.

When a mismatched guanine or cytosine is positioned opposite to A^T, further destabilization of the modified duplexes by an average of 8°C can be observed. Surprisingly, the positioning of an adenine opposite of A^T results in virtually no change in melting temperatures (<1°C) compared to the duplexes with the thymine-A^T base pair. In contrast, an adenine–adenine mismatch in the three unmodified duplexes leads to an average drop in melting temperature of 14°C in comparison to the natural adenine–thymine pair (data not shown). This suggests that A^T is capable of forming equally stable base pairs with thymine and adenine.

The quantum yields of the duplexes containing a guanine-A^T mismatch increase between 13 and 36% in comparison to the normal matched modified duplexes and the corresponding values for cytosine-A^T mismatches are 0 and 36%. For the adenine-A^T base pair a decrease in quantum yield between 0 and 27% is observed. However, we calculated up to 16% of the duplexes to be denatured at the temperature at which these measurements were performed (25°C). Taking into account this and experimental errors when measuring low-quantum yields, the changes are fairly low and should not be over-interpreted. Furthermore, when comparing the spectral shape and emission maxima as well as CD-spectra of the various mismatched duplexes to that of the corresponding matched duplexes, virtually no changes can be observed (data not shown).

Computation of the internal wobble of A^T in DNA. To estimate the internal motion of A^T inside the base stack of DNA, anisotropy measurements were recorded for two of the modified duplexes, **AA** and *TA* (Table 1), which were prepared in phosphate buffer (500 mM Na$^+$, pH 7.5) of high viscosity (65 and 77.2% sucrose w/v). The high viscosity hinders motion of the DNA helices in between the moment of excitation and emission. In standard phosphate buffer (500 mM Na$^+$, pH 7.5) anisotropy values of 0.30 and 0.21 were recorded for samples **AA** and *TA*, respectively. When performing the same

Table 2. Comparison of the melting temperatures and quantum yields of duplexes containing a mismatched base opposite of A^T with its matched counterparts

Neighbouring bases = name of oligonucleotide[a]	Base opposite A^{Ta}	$T_m^{A^T}$ mismatch (−°C)[b]	$T_m^{A^T}$ (−°C)[b]	ΔT_m (−°C)	$\Phi_{f\ mismatch}$[b,c]	$\Phi_f^{A^T}$[b,c]
GA	G	36		−7	0.009	0.008
	C	36	43	−7	0.010	
	A	43		0	0.008	
CT	G	36		−9	0.006	0.005
	C	36	45	−9	0.005	
	A	46		1	0.004	
CA	G	36		−7	0.015	0.011
	C	36	43	−7	0.015	
	A	42		−1	0.008	

[a]Oligonucleotides are named using the two bases neighbouring A^T. Full sequences can be found in Table 1. The base opposite A^T in the duplexes is replaced by the three other bases that normally do not base-pair with adenine (G, C, A).
[b]Samples were prepared in phosphate buffer (500 mM Na$^+$, pH 7.5) at a duplex concentration of 2.5 μM.
[c]Fluorescence quantum yields were determined relative to the reference quinine sulphate in 0.5 M H$_2$SO$_4$ (Φ_f = 0.55) and are averages of at least two independent measurements.

measurements in high-viscosity buffer, a limiting anisotropy of on average 0.34 was measured for both samples, **AA** and *TA*. The difference between the values measured at 65 and 77.2% sucrose (w/v) was within experimental error. The limiting anisotropy recorded here is lower than the fundamental anisotropy that was recorded for the A^T monomer in a vitrified matrix (0.38). The difference in the anisotropy in DNA in viscous solution and the monomer in a vitrified matrix is a result of motions of A^T inside the base-stack and calculations (51) suggest an internal wobble of 16 degrees.

Photophysical characterization of A^T in DNA context

Fluorescence properties of A^T in single-stranded DNA. The fluorescence properties of A^T upon incorporation into the 10 single-stranded oligonucleotides (listed in Table 1) are shown in Table 3. These data show no large shift in the emission maxima (351–358 nm) in comparison to the free A^T-monomer (354 nm). Furthermore, when comparing the emission spectra of the various modified oligonucleotides to that of the monomer A^T and the corresponding modified duplex, only minimal changes in the spectral envelope can be observed (data not shown).

The fluorescence quantum yields for the 10 modified oligonucleotides range between 0.005 and 0.21 (Table 3). The **AA** sequence shows the highest quantum yield (0.21). In general, with exception of **GA**, the highest quantum yields are observed for the sequences with an adenine flanking A^T at the 3′-side (**AA**, *CA*, *TA*). Lower quantum yields are observed for a cytosine 3′ of A^T (**GC**, *AC*, *CC*) and these values decrease further for having a thymine (*CT*) and finally a guanine 3′ of A^T (*TG*, **GG**). Not surprisingly, the lowest quantum yield (0.005) was found for the sequence with two guanines (**GG**) neighbouring A^T. The average quantum yield (0.051) is approximately 12 times lower for the modified oligonucleotides in comparison to the free A^T-monomer (0.61).

Average lifetimes of A^T incorporated into the 10 modified oligonucleotides listed in Table 1 range between 0.9 and 2.0 ns. Fluorescence intensity decays were fitted to three lifetimes for all samples, except for strands **AA** and **GC**, which showed a mono-exponential decay. For all strands, except for **GC** (τ = 2.0 ns), the average lifetime of the incorporated A^T is lower than the lifetime of the A^T monomer in water (1.8 ns).

Fluorescence properties of A^T in double-stranded DNA. The fluorescence properties of the A^T-monomer when incorporated into duplex DNA, consisting of the modified sequences (listed in Table 1) with their unmodified complement are shown in Table 4. The emission maxima for the modified duplexes (349–354 nm) are virtually not shifted in comparison to the A^T-monomer (354 nm) and the modified single strands (351–358 nm).

The fluorescence quantum yields that were measured for the 10 modified duplexes range between 0.050 and 0.003 (Table 4). Analogous to the quantum yields for the

Table 3. Wavelengths of emission maxima and quantum yields of the ten A^T-modified single strands

Oligonucleotide[a]	Em$_{max}$ (nm)	Φ_f[b]
AA	353	0.21
CA	351	0.090
TA	352	0.076
GC	358	0.042
AC	357	0.031
CC	355	0.021
GA	353	0.018
CT	358	0.014
TG	355	0.006
GG	355	0.005

[a]Oligonucleotides are named by the two bases neighbouring A^T. Full sequences can be found in Table 1.
[b]Fluorescence quantum yields were determined relative to the reference quinine sulphate in 0.5 M H_2SO_4 (Φ_f = 0.55) at an excitation wavelength of 300 nm and are averages of three independent measurements. Samples were prepared in phosphate buffer (500 mM Na^+, pH 7.5).

Table 4. Wavelength of emission maxima and quantum yields of the ten A^T-modified double-strands

Oligonucleotides[a]	Em$_{max}$ (nm)	Φ_f[b]
AA	350	0.050
TA	353	0.016
CA	354	0.011
AC	349	0.009
GA	351	0.008
CT	351	0.005
GC	351	0.005
CC	352	0.004
TG	351	0.003
GG	354	0.003

[a]Oligonucleotides are named by the two bases neighbouring A^T. Full sequences can be found in Table 1.
[b]Fluorescence quantum yields were determined relative to the reference quinine sulphate in 0.5 M H_2SO_4 (Φ_f = 0.55) and are averages of at least two independent measurements. Samples were prepared in phosphate buffer (500 mM Na^+, pH 7.5) at a duplex concentration of 2.5 μM.

single-stranded oligonucleotides, sequence **AA** shows the highest quantum yield. Furthermore, the observation that an adenine 3′ of A^T (**AA**, *TA*, *CA*) yields the highest fluorescence (with exception of **GA**) and a guanine 3′ of A^T (*TG*, **GG**) yields the lowest quantum yield is found also for the duplex case. As for the single strands, sequence **GG** shows the lowest quantum yield in the duplex. The average quantum yield of A^T incorporated into duplexes (0.011) is reduced ~5-fold in comparison to the average quantum yield of the single strands (0.051).

Average lifetimes of A^T incorporated into the 10 modified duplexes vary between 0.2 and 1.2 ns. All fluorescence intensity decays for these samples were fitted to three fluorescence lifetimes. For all duplexes, the average lifetimes of A^T are lower than the lifetime of the A^T monomer in water. Also when compared to the corresponding lifetimes of A^T in single-stranded oligonucleotides, these lifetime values are lower except for strands **GG**, *TG* and **GA**.

DISCUSSION

In a recent study, we characterized a novel series of 8-substituted adenosine analogues. That investigation revealed promising features for triazole adenine (A^T) such as a high-quantum yield and a red-shifted absorption band, allowing specific excitation outside the DNA-absorption band (49). In the study presented here we therefore decided to synthesize the 2′-deoxyribose derivative of A^T in order to perform a comprehensive photophysical and structural characterization when A^T is incorporated into DNA.

Structure and stability of DNA duplexes containing A^T

To investigate the influence on B-DNA stability after incorporation of A^T, we performed UV-melting experiments on the 10 different 10-mer duplexes. These sequences contain one A^T flanked by varying combinations of purines and pyrimidines as direct 3′ and 5′ neighbours. The resulting melting data show a moderate destabilization of duplexes containing A^T by an average drop in melting temperature of 8°C compared to the natural duplexes. The decrease in stability is dependent on the bases surrounding A^T. A more thorough investigation shows that duplexes containing a pyrimidine 3′ of A^T are the most stable. This is most likely due to a better stacking between A^T and the surrounding bases when it is flanked by a pyrimidine as a 3′ neighbour. The general destabilization is most probably caused by steric clashes of the substituent triazole ring and pentyl chain in the 8-position of A^T with the phosphate backbone and sugar moieties. This steric clash would account for a considerable energy cost if the base is to be accommodated in the duplex in its *anti* conformation.

Similar observations have been made for 8-methoxy and 8-bromo substituted adenine, which showed an average destabilization of 6°C in 11-mer DNA duplexes (1.0 M NaCl, pH 7, 0.010 M phosphate, 0.001 M EDTA) (54). It has also been shown previously that many 8-substituted purines show a preference for the *syn* conformation (55,56). However, calculations suggested a *syn/anti* equilibrium to be present in DNA helices for other analogues (57). The preferred orientation of the modified base around the glycosidic bond in duplex DNA depends on the hydrogen bonding preferences, which can change depending on the bulky substituent and can improve the relative stability of Hoogsteen pairs. Stabilization of the *syn* orientation compared to the *anti* orientation helps to explain the mutagenicity of bulky DNA adducts. In the case of the A^T(*anti*).T base pair the triazole moiety would have strong unfavourable steric and electrostatic interactions with the adjacent phosphodiester backbone, whereas in the A^T(*syn*) orientation there is the possibility of a third weakly stabilizing C-H—O hydrogen bond to thymine (58). In both versions of the A^T.T base pair, the pentyl group will project into the aqueous environment and this could lead to entropic destabilization.

Despite this possible change in conformation, A^T still shows base pairing capacity to thymine and seems to be stacked reasonably well in the DNA duplex in that case. This can be concluded from a limiting anisotropy value of 0.34 which was recorded for A^T in duplexes **AA** and **TA** in viscous sucrose solutions. The difference compared to the fundamental anisotropy of A^T in a vitrified matrix (0.38) was calculated to be due to an internal wobble of A^T in the DNA duplex of 16°. This value is higher than the estimated wobble for the natural canonical bases (∼5°), but lower than the corresponding value for the intercalating dye ethidium bromide (21°) (51). Furthermore, melting experiments were performed to examine the base pairing specificity of A^T. Three of the modified sequences (**GA**, **CT**, **CA**) were annealed with strands containing an adenine, guanine or cytosine opposite of A^T instead of a thymine. Melting temperatures recorded for A^T-cytosine/guanine mismatches reveal an average drop in melting temperatures of 16°C, almost twice as large compared to an A^T-thymine match (8°C). The A^T-cytosine/guanine mismatch melting temperatures are in line with the average destabilization (14°C) recorded for a single-base mismatch of adenine–adenine in these duplexes compared to their natural matching counterparts. It is therefore reasonable to assume that A^T exhibits some hydrogen-bonding with thymine but shows virtually no base-pairing with guanine or cytosine. Surprisingly, the same mismatch experiment performed for an A^T-adenine mismatch showed on average no further destabilization of the duplexes (8°C) compared to the A^T-thymine case. This suggests that A^T is able to form equally strong base pairs with thymine and adenine. To the best of our knowledge, no similar findings have been previously reported for other adenine analogues. The putative A^T.A base pair in Figure 6 would have a similar overall shape to a Watson–Crick base pair and would have good stacking interactions with surrounding base pairs and, thus, constitutes a plausible structure. Protonation of N(1) of adenine would provide a second hydrogen bond. Additionally a possible third weakly stabilizing C-H—N hydrogen bond to H(2) on adenine may be formed (58). It should be mentioned that the pKa of N(1) of adenine is approximately 4.0. However, in double-stranded DNA, if it is or has the possibility of being involved in H-bonding, it can be raised much higher. Thus, the proposed base pair structure is presently speculative and future high-resolution structural studies will be
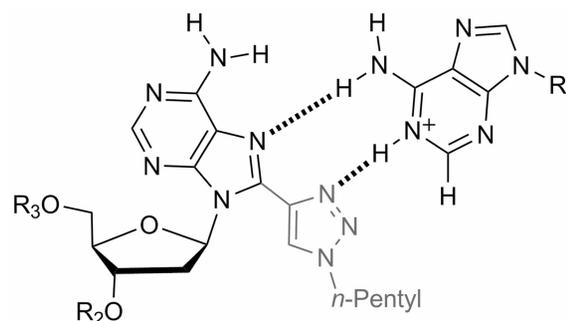

Figure 6. Putative stabilized A^T.A base pair. Only the sugar attached to A^T is shown and its triazole and pentyl chain are coloured grey. R_1, R_2 and R_3 represent the rest of the DNA structure.

necessary to accurately determine the base pairing properties of A^T.

As was mentioned above, bulky DNA adducts can influence the hydrogen bonding preferences of the base, resulting in potential mispairing involving the Hoogsteen face. Deviations in the base pairing specificity have also been found for other base analogues due to the introduced modifications to the natural base. The adenine analogue 2-aminopurine is, for example, able to form base pairs both with thymine and cytosine (28,59). Furthermore, the base discriminating fluorescent analogue BPP can form stable base pairs both with adenine and guanine (7).

The drop in melting temperature caused by A^T (8°C) is not dramatic when compared to most other fluorescent base analogues which have been incorporated into DNA. For example, earlier observations for decamers containing the fluorescent analogue 2-aminopurine have shown a drop in stability of 10°C (0.1 M KCl, 0.1 mM EDTA, 21 μM DNA duplexes) (27). In another study involving 14-mer duplexes a decrease of 6°C in melting temperature was observed after incorporation of 2-aminopurine in place of adenine (0.015 M sodium citrate, pH 7.25, 50 μM DNA duplexes) (60). However, in a recent study, a decrease in melting temperature of merely 3.5°C was recorded for 13-mer duplexes (10 mM Na_2HPO_4/NaH_2PO_4, 150 mM NaCl, pH 6.5, 11.9 μM DNA duplexes) (61). Besides 2-aminopurine, other adenine analogues such as 6MAP and DMAP on average have shown a slight (2.4°C) to moderate destabilization (4.6°C) in 21-mer duplexes (10 mM Tris, pH 7.5, with 10 mM NaCl), respectively (16). Furthermore, the pteridine guanine analogue 3-MI shows an average drop in melting temperature (8.3°C) comparable to a single-base mismatch under similar conditions (15).

Importantly, the CD-spectra recorded for the different duplexes containing A^T show a general signature for regular B-form DNA. This means that the A^T-modification does not perturb the overall B-form of the DNA. Five of the modified duplexes (*CT*, *CA*, *TG*, *CC* and **AA**) show an almost identical CD-spectrum to their corresponding natural duplexes. Surprisingly, no change in CD signal was found for the duplexes **AA** and *CT* in the region where only the A^T absorption bands are situated. Similar findings have been reported in the case of tC^o and currently we have no satisfactory explanation for this phenomenon (23). Duplexes *CA*, *TG* and *CC* show slight differences which correspond well to the A^T- absorption bands. In contrast, the other duplexes show more distinct differences compared to the CD-signature of their corresponding natural duplexes (**GA**, **G***C*, **GG**, *TA* and *AC*). For the duplexes **GA**, **G***C* and **GG**, the CD is most perturbed, which may indicate that the B-DNA structure is more distorted when A^T is flanked by a guanine at the 5′-side. As expected, the deviations in CD signals correspond well to the absorption difference of A^T and A in duplex DNA. Comparable results were found for the CD spectra of duplexes containing the fluorescent analogue tC (62). Also the adenine analogue, 2-aminopurine, shows a particular significant CD-band >300 nm when incorporated into duplex DNA, whereas

minor differences in CD-signal can be detected where the regular DNA bases absorb (60,63).

Fluorescence properties of A^T in single- and double-stranded DNA

The emission maximum and the spectral envelope of A^T are virtually unaffected by incorporation into oligonucleotides. On the other hand, as reported for virtually all base analogues (5,15,16,24,26), incorporation of A^T in oligonucleotides causes a significant drop in fluorescence quantum yield. Quantum yield values for A^T in single-stranded DNA (0.005–0.21) are on average 12 times lower than those recorded for the A^T monomer in water (0.61). These values are reduced approximately another five times in duplexes (0.003–0.050). Furthermore, the average lifetimes of A^T in both single- (0.9–1.5 ns; except **G***C*: $<\tau> = 2$ ns) and double-stranded DNA (0.2–1.2 ns) are also reduced compared to the lifetime of the A^T monomer in water (1.8 ns). With exception of the single-stranded samples **AA** and **G***C*, showing a mono-exponential decay, three lifetimes were recorded for A^T incorporated in all double- and single-stranded samples. These changes in photophysical properties when going from monomer A^T to DNA-incorporated A^T may be explained by different levels of stacking and, thus, electronic interaction with other bases in DNA. For both the single- and double-stranded samples an increase in the non-radiative rate constant (k_{nr}) as well as a decrease in the radiative rate constant (k_f) of A^T can be observed compared to its free monomeric form (data not shown). First of all, the absorption of A^T is most likely decreased in DNA compared to the free monomer, as seen for all natural bases, due to stacking interactions with the surrounding bases. As a result the radiative rate constant, k_f, is lowered and gets influenced by the reduction of the extinction coefficient since they are related through the Strickler–Berg equation (64). This corresponds well with the drop in quantum yield and decrease in k_f (except for strand *AC*) which we observed for the duplex samples compared to the single strands. Second, several conformations of A^T might be present in DNA. Calculations suggest that an increase in the dihedral angle between the triazole ring and the adenine moiety (ω), starting from a planar conformation ($\omega = 0$), results in a blueshifted absorption and decreased oscillator strength of the lowest electronic transition (49) (B. Albinsson, personal communication). It was previously suggested by looking at the orbital diagrams of the model compound 9-methyl-8-(1*H*-1,2,3-triazol-4-yl)adenine that the single bond character of the bond between the adenine and triazole moiety of A^T gains bond order in the excited state, resulting in a planar excited state (49). However, in DNA A^T might be forced to remain in a twisted geometry in the excited state which also results in changes in oscillator strength compared to the monomer A^T, corresponding to different geometries of A^T around the dihedral bond. Again, since oscillator strength is proportional to the radiative rate constant (k_f) of the excited state through the Strickler–Berg equation (64), these

different emitting species may also explain the multiple fluorescence lifetimes observed. Finally, changes in photophysical properties can also be explained by increases in k_{nr} upon incorporation of A^T in oligonucleotides as a result of, for example, photoinduced electron transfer from neighbouring bases, as will be further described below.

Not only we do notice a general decrease in quantum yield upon incorporation of A^T into DNA, but also significant variations in fluorescence are observed when A^T is placed in various sequence contexts. This is a common property of many fluorescent base analogues (15,16,65–67). Sequence **AA**, with two adenines neighbouring A^T, shows the highest quantum yield value both for single- (0.21) and double-stranded DNA (0.05). Quantum yield values decrease for having an adenine (*CA*, *TA*, exception: **GA**), a cytosine (**G**C, **A**C, *CC*) or a thymine (*CT*) flanking A^T on the 3′-side. The lowest quantum yield values are detected in the case where A^T is flanked with two guanines (**GG**; 0.005 ss; 0.003 ds) or with a guanine at the 3′-side (*TG*; 0.006 ss; 0.003 ds). This is not surprising, since guanine has the lowest oxidation potential of all natural bases (68) and therefore might transfer an electron into the neighbouring A^T resulting in a fast relaxation to the ground state. This kind of quenching pattern has been seen before both for the base discriminating analogue BPP and 2-aminopurine when flanked by a guanine (7,66). However, sequences that have a guanine neighbouring A^T at the 5′-side (**GC** and **GA**) show significantly higher quantum yields (0.042 and 0.018, respectively). This corresponds to previous observations made for the fluorescent base analogue tC°, namely that both proximity to a guanine and structural differences are important for quenching (23). These structural differences probably include parameters such as relative orientation and stacking of A^T and neighbouring guanines.

Finally, it is important to note that the maximum quantum yield recorded for A^T in single strands (0.21, **AA**) is approximately 10 times higher than the maximum value measured for the widely used dye 2-aminopurine. Furthermore, the maximum quantum yield of A^T when incorporated into duplexes is approximately five times higher than the corresponding value for 2-aminopurine. It should also be noted that good lines of evidence suggest that these values for 2-aminopurine are overestimations since in some cases 2-aminopurine was incorporated at the ends of the oligonucleotide (26). Moreover, the maximum quantum yield values for A^T in single-stranded DNA reported here are also five and two times higher, respectively, than for the pteridine adenine analogues 6MAP (0.041) and DMAP (0.11) under similar conditions (16). In duplexes, the fluorescence of 6MAP and DMAP is quenched by an additional 2% compared to the monomer fluorescence quantum yield. Furthermore the brightness ($\sim\Phi_f \times \varepsilon$) of A^T in duplex DNA is approximately three times higher than for 2-aminopurine and essentially the same as for 6MAP when comparing with extinction in the lowest energy absorption band (16,26,63).

CONCLUSION

We have performed a comprehensive photophysical and structural characterization of the 2′-deoxyribose derivative of A^T incorporated into DNA and in its monomeric form and have found very promising properties of A^T compared to the widely used commercially available 2-aminopurine. A^T causes only minimal structural perturbations to B-DNA. Furthermore, A^T has a very high-quantum yield as a monomer in water (0.61) as well as in methanol (0.49). Inside DNA, the quantum yield reaches values >20% in certain single strands and 5% in double strands, 10 to 5 times higher, respectively, than corresponding values for 2-aminopurine. These promising features should lead to future applications of A^T in studies concerning the structure, dynamics and interactions of nucleic acids.

SUPPLEMENTARY DATA

Supplementary Data are available at NAR Online.

REFERENCES

1. Sinkeldam,R.W., Greco,N.J. and Tor,Y. (2010) Fluorescent analogs of biomolecular building blocks: design, properties, and applications. *Chem. Rev.*, **110**, 2579–2619.
2. Greco,N.J. and Tor,Y. (2005) Simple fluorescent pyrimidine analogues detect the presence of DNA abasic sites. *J. Am. Chem. Soc.*, **127**, 10784–10785.
3. Srivatsan,S.G., Greco,N.J. and Tor,Y. (2008) A highly emissive fluorescent nucleoside that signals the activity of toxic ribosome-inactivating proteins. *Angew. Chem., Int. Ed. Engl.*, **47**, 6661–6665.
4. Srivatsan,S.G., Weizman,H. and Tor,Y. (2008) A highly fluorescent nucleoside analog based on thieno 3,4-d pyrimidine senses mismatched pairing. *Org. Biomol. Chem.*, **6**, 1334–1338.
5. Berry,D.A., Jung,K.Y., Wise,D.S., Sercel,A.D., Pearson,W.H., Mackie,H., Randolph,J.B. and Somers,R.L. (2004) Pyrrolo-dC and pyrrolo-C: fluorescent analogs of cytidine and 2′-deoxycytidine for the study of oligonucleotides. *Tetrahedron Lett.*, **45**, 2457–2461.
6. Dodd,D.W., Swanick,K.N., Price,J.T., Brazeau,A.L., Ferguson,M.J., Jones,N.D. and Hudson,R.H.E. (2010) Blue fluorescent deoxycytidine analogues: convergent synthesis,

solid-state and electronic structure, and solvatochromism. *Org. Biomol. Chem.*, **8**, 663–666.

7. Okamoto,A., Saito,Y. and Saito,I. (2005) Design of base-discriminating fluorescent nucleosides. *J. Photochem. Photobiol. C*, **6**, 108–122.

8. Okamoto,A., Tainaka,K. and Saito,I. (2003) Clear distinction of purine bases on the complementary strand by a fluorescence change of a novel fluorescent nucleoside. *J. Am. Chem. Soc.*, **125**, 4972–4973.

9. Okamoto,A., Tainaka,K. and Saito,I. (2003) Synthesis and properties of a novel fluorescent nucleobase, naphthopyridopyrimidine. *Tetrahedron Lett.*, **44**, 6871–6874.

10. Okamoto,A., Tanaka,K., Fukuta,T. and Saito,I. (2003) Design of base-discriminating fluorescent nucleoside and its application to T/C SNP typing. *J. Am. Chem. Soc.*, **125**, 9296–9297.

11. Okamoto,A., Tainaka,K. and Saito,I. (2003) Detection of A/G single nucleotide alteration in RNA using base-discriminating fluorescent oligodeoxynucleotides. *Chem. Lett.*, **32**, 684–685.

12. Hawkins,M.E. (2001) Fluorescent pteridine nucleoside analogs - A window on DNA interactions. *Cell. Biochem. Biophys.*, **34**, 257–281.

13. Hawkins,M.E. and Balis,F.M. (2004) Use of pteridine nucleoside analogs as hybridization probes. *Nucleic Acids Res.*, **32**, e62.

14. Driscoll,S.L., Hawkins,M.E., Balis,F.M., Pfleiderer,W. and Laws,W.R. (1997) Fluorescence properties of a new guanosine analog incorporated into small oligonucleotides. *Biophys. J.*, **73**, 3277–3286.

15. Hawkins,M.E., Pfleiderer,W., Balis,F.M., Porter,D. and Knutson,J.R. (1997) Fluorescence properties of pteridine nucleoside analogs as monomers and incorporated into oligonucleotides. *Anal. Biochem.*, **244**, 86–95.

16. Hawkins,M.E., Pfleiderer,W., Jungmann,O. and Balis,F.M. (2001) Synthesis and fluorescence characterization of pteridine adenosine nucleoside analogs for DNA incorporation. *Anal. Biochem.*, **298**, 231–240.

17. Zhao,Y. and Baranger,A.M. (2003) Design of an adenosine analogue that selectively improves the affinity of a mutant U1A protein for RNA. *J. Am. Chem. Soc.*, **125**, 2480–2488.

18. Zhao,Y., Knee,J.L. and Baranger,A.M. (2008) Characterization of two adenosine analogs as fluorescence probes in RNA. *Bioorg. Chem.*, **36**, 271–277.

19. Seela,F. and Zulauf,M. (1998) 7-deazaadenine-DNA: bulky 7-iodo substituents or hydrophobic 7-hexynyl chains are well accommodated in the major groove of oligonucleotide duplexes. *Chem. Eur. J.*, **4**, 1781–1790.

20. Seela,F., Zulauf,M., Sauer,M. and Deimel,M. (2000) 7-substituted 7-deaza-2′-deoxyadenosines and 8-aza-7-deaza-2′-deoxyadenosines: fluorescence of DNA-base analogues induced by the 7-alkynyl side chain. *Helv. Chim. Acta*, **83**, 910–927.

21. Börjesson,K., Preus,S., El-Sagheer,A.H., Brown,T., Albinsson,B. and Wilhelmsson,L.M. (2009) Nucleic acid base analog FRET-pair facilitating detailed structural measurements in nucleic acid containing systems. *J. Am. Chem. Soc.*, **131**, 4288–4293.

22. Preus,S., Börjesson,K., Kilså,K., Albinsson,B. and Wilhelmsson,L.M. (2010) Characterization of nucleobase analogue FRET acceptor tC(nitro). *J. Phys. Chem. B*, **114**, 1050–1056.

23. Sandin,P., Börjesson,K., Li,H., Mårtensson,J., Brown,T., Wilhelmsson,L.M. and Albinsson,B. (2008) Characterization and use of an unprecedentedly bright and structurally non-perturbing fluorescent DNA base analogue. *Nucleic Acids Res.*, **36**, 157–167.

24. Wilhelmsson,L.M. (2010) Fluorescent nucleic acid base analogues. *Q. Rev. Biophys.*, **43**, 159–183.

25. Dodd,D.W. and Hudson,R.H.E. (2009) Intrinsically fluorescent base-discriminating nucleoside analogs. *Mini-Rev. Org. Chem.*, **6**, 378–391.

26. Ward,D.C., Reich,E. and Stryer,L. (1969) Fluorescence studies of nucleotides and polynucleotides. *J. Biol. Chem.*, **244**, 1228–1237.

27. Nordlund,T.M., Xu,D. and Evans,K.O. (1994) DNA melting, premelting and dynamics measured by optical spectroscopy of normal and fluorescent bases. *Biophys. J.*, **66**, A231–A231.

28. Sowers,L.C., Boulard,Y. and Fazakerley,G.V. (2000) Multiple structures for the 2-aminopurine-cytosine mispair. *Biochemistry*, **39**, 7613–7620.

29. Law,S.M., Eritja,R., Goodman,M.F. and Breslauer,K.J. (1996) Spectroscopic and calorimetric characterizations of DNA duplexes containing 2-aminopurine. *Biochemistry*, **35**, 12329–12337.

30. Rist,M.J. and Marino,J.P. (2002) Fluorescent nucleotide base analogs as probes of nucleic acid structure, dynamics and interactions. *Curr. Org. Chem.*, **6**, 775–793.

31. Wilson,J.N. and Kool,E.T. (2006) Fluorescent DNA base replacements: reporters and sensors for biological systems. *Org. Biomol. Chem.*, **4**, 4265–4274.

32. Sandin,P., Stengel,G., Ljungdahl,T., Börjesson,K., Macao,B. and Wilhelmsson,L.M. (2009) Highly efficient incorporation of the fluorescent nucleotide analogs tC and tC(O) by Klenow fragment. *Nucleic Acids Res.*, **37**, 3924–3933.

33. Stengel,G., Gill,J.P., Sandin,P., Wilhelmsson,L.M., Albinsson,B., Nordén,B. and Millar,D. (2007) Conformational dynamics of DNA polymerase probed with a novel fluorescent DNA base analogue. *Biochemistry*, **46**, 12289–12297.

34. Stengel,G., Urban,M., Purse,B.W. and Kuchta,R.D. (2009) High density labeling of polymerase chain reaction products with the fluorescent base analogue tCo. *Anal. Chem.*, **81**, 9079–9085.

35. Stengel,G., Urban,M., Purse,B.W. and Kuchta,R.D. (2010) Incorporation of the fluorescent ribonucleotide analogue tCTP by T7 RNA polymerase. *Anal. Chem.*, **82**, 1082–1089.

36. Srivatsan,S.G. and Tor,Y. (2007) Fluorescent pyrimidine ribonucleotide: synthesis, enzymatic incorporation, and utilization. *J. Am. Chem. Soc.*, **129**, 2044–2053.

37. Liu,C. and Martin,C.T. (2002) Promoter clearance by T7 RNA polymerase - initial bubble collapse and transcript dissociation monitored by base analog Fluorescence. *J. Biol. Chem.*, **277**, 2725–2731.

38. Liu,C. and Martin,C.T. (2001) Fluorescence characterization of the transcription bubble in elongation complexes of T7 RNA polymerase. *J. Mol. Biol.*, **308**, 465–475.

39. Baker,R.P. and Reha-Krantz,L.J. (1998) Identification of a transient excision intermediate at the crossroads between DNA polymerase extension and proofreading pathways. *Proc. Natl Acad. Sci. USA*, **95**, 3507–3512.

40. Bandwar,R.P. and Patel,S.S. (2001) Peculiar 2-aminopurine fluorescence monitors the dynamics of open complex formation by bacteriophage T7 RNA polymerase. *J. Biol. Chem.*, **276**, 14075–14082.

41. Beechem,J.M., Otto,M.R., Bloom,L.B., Eritja,R., Reha-Krantz,L.J. and Goodman,M.F. (1998) Exonuclease-polymerase active site partitioning of primer-template DNA strands and equilibrium Mg^{2+} binding properties of bacteriophage T4 DNA polymerase. *Biochemistry*, **37**, 10144–10155.

42. Frey,M.W., Sowers,L.C., Millar,D.P. and Benkovic,S.J. (1995) The nucleotide analog 2-aminopurine as a spectroscopic probe of nucleotide incorporation by the Klenow fragment of Escherichia-Coli polymerase-I and bacteriophage-T4 DNA-polymerase. *Biochemistry*, **34**, 9185–9192.

43. Hochstrasser,R.A., Carver,T.E., Sowers,L.C. and Millar,D.P. (1994) Melting of a DNA helix terminus within the active-site of a DNA-polymerase. *Biochemistry*, **33**, 11971–11979.

44. Ujvari,A. and Martin,C.T. (1996) Thermodynamic and kinetic measurements of promoter binding by T7 RNA polymerase. *Biochemistry*, **35**, 14574–14582.

45. Deprez,E., Tauc,P., Leh,H., Mouscadet,J.F., Auclair,C., Hawkins,M.E. and Brochon,J.C. (2001) DNA binding induces dissociation of the multimeric form of HIV-1 integrase: a time-resolved fluorescence anisotropy study. *Proc. Natl Acad. Sci. USA*, **98**, 10090–10095.

46. Stephens,O.M., Yi-Brunozzi,H.Y. and Beal,P.A. (2000) Analysis of the RNA-editing reaction of ADAR2 with structural and fluorescent analogues of the GluR-B R/G editing site. *Biochemistry*, **39**, 12243–12251.

47. Yi-Brunozzi,H.Y., Stephens,O.M. and Beal,P.A. (2001) Conformational changes that occur during an RNA-editing adenosine deamination reaction. *J. Biol. Chem.*, **276**, 37827–37833.

48. Sandin,P., Tumpane,J., Börjesson,K., Wilhelmsson,L.M., Brown,T., Nordén,B., Albinsson,B. and Lincoln,P. (2009) Thermodynamic aspects of DNA nanoconstruct stability and design. *J. Phys. Chem. C*, **113**, 5941–5946.

49. Dyrager,C., Börjesson,K., Diner,P., Elf,A., Albinsson,B., Wilhelmsson,L.M. and Grøtli,M. (2009) Synthesis and photophysical characterisation of fluorescent 8-(1H-1,2,3-triazol-4-yl)adenosine derivatives. *Eur. J. Org. Chem.*, 1515–1521.

50. Melhuish,W.H. (1961) Quantum efficiencies of fluorescence of organic substances - effect of solvent and concentration of fluorescent solute. *J. Phys. Chem.*, **65**, 229–235.

51. Barkley,M.D. and Zimm,B.H. (1979) Theory of twisting and bending of chain macromolecules - analysis of the fluorescence depolarization of DNA. *J. Chem. Phys.*, **70**, 2991–3007.

52. Ikehara,M. and Kaneko,M. (1970) Studies of nucleosides and nucleotides–XLI: purine cyclonucleosides-8 selective sulfonylation of 8-bromoadenosine derivatives and an alternate synthesis of 8,2′- and 8,3′-S-cyclonucleosides. *Tetrahedron*, **26**, 4251–4259.

53. O'Mahony,G., Ehrman,E. and Grøtli,M. (2008) Synthesis and photophysical properties of novel cyclonucleosides - substituent effects on fluorescence emission. *Tetrahedron*, **64**, 7151–7158.

54. Eason,R.G., Burkhardt,D.M., Phillips,S.J., Smith,D.P. and David,S.S. (1996) Synthesis and characterization of 8-methoxy-2′-deoxyadenosine-containing oligonucleotides to probe the syn glycosidic conformation of 2′-deoxyadenosine within DNA. *Nucleic Acids Res.*, **24**, 890–897.

55. Sarma,R.H., Lee,C.H., Evans,F.E., Yathindr,N. and Sundaral,M. (1974) Probing interrelation between glycosyl torsion, sugar pucker, and backbone conformation in C(8) substituted adenine-nucleotides by H-1 and H-1-P-31 fast fourier-transform nuclear magnetic-resonance methods and conformational energy calculations. *J. Am. Chem. Soc.*, **96**, 7337–7348.

56. Tavale,S.S. and Sobell,H.M. (1970) Crystal and molecular structure of 8-bromoguanosine and 8-bromoadenosine, 2 purine nucleosides in *syn* conformation. *J. Mol. Biol.*, **48**, 109–123.

57. Millen,A.L., Manderville,R.A. and Wetmore,S.D. (2010) Conformational flexibility of C8-Phenoxyl-2′-deoxyguanosine nucleotide adducts. *J. Phys. Chem. B*, **114**, 4373–4382.

58. Leonard,G.A., McAuleyhecht,K., Brown,T. and Hunter,W.N. (1995) Do C-H...O hydrogen-bonds contribute to the stability of nucleic-acid base-pairs? *Acta Crystallogr. Sect. D-Biol. Crystallogr.*, **51**, 136–139.

59. Sowers,L.C., Fazakerley,G.V., Eritja,R., Kaplan,B.E. and Goodman,M.F. (1986) Base-pairing and mutagenesis - observation of a protonated base pair between 2-aminopurine and cytosine in an oligonucleotide by proton NMR. *Proc. Natl Acad. Sci. USA*, **83**, 5434–5438.

60. Petrauskene,O.V., Schmidt,S., Karyagina,A.S., Nikolskaya,II., Gromova,E.S. and Cech,D. (1995) The interaction of DNA duplexes containing 2-aminopurine with restriction endonucleases EcoRII and SsoII. *Nucleic Acids Res.*, **23**, 2192–2197.

61. Dallmann,A., Dehmel,L., Peters,T., Mugge,C., Griesinger,C., Tuma,J. and Ernsting,N.P. (2010) 2-Aminopurine incorporation perturbs the dynamics and structure of DNA. *Angew. Chem. Int. Edit.*, **49**, 5989–5992.

62. Engman,K.C., Sandin,P., Osborne,S., Brown,T., Billeter,M., Lincoln,P., Nordén,B., Albinsson,B. and Wilhelmsson,L.M. (2004) DNA adopts normal B-form upon incorporation of highly fluorescent DNA base analogue tC: NMR structure and UV-Vis spectroscopy characterization. *Nucleic Acids Res.*, **32**, 5087–5095.

63. Johnson,N.P., Baase,W.A. and von Hippel,P.H. (2004) Low-energy circular dichroism of 2-aminopurine dinucleotide as a probe of local conformation of DNA and RNA. *Proc. Natl Acad. Sci. USA*, **101**, 3426–3431.

64. Strickler,S.J. and Berg,R.A. (1962) Relationship between absorption intensity and fluorescence lifetime of molecules. *J. Chem. Phys.*, **37**, 814–822.

65. Narayanan,M., Kodali,G., Xing,Y.J., Hawkins,M.E. and Stanley,R.J. (2010) Differential fluorescence quenching of fluorescent nucleic acid base analogues by native nucleic acid monophosphates. *J. Phys. Chem. B*, **114**, 5953–5963.

66. Somsen,O.J.G., Hoek,v.A. and Amerongen,v.H. (2005) Fluorescence quenching of 2-aminopurine in dinucleotides. *Chem. Phys. Lett.*, **402**, 61–65.

67. Wilson,J.N., Cho,Y.J., Tan,S., Cuppoletti,A. and Kool,E.T. (2008) Quenching of fluorescent nucleobases by neighboring DNA: The "Insulator" concept. *ChemBioChem*, **9**, 279–285.

68. Fukuzumi,S., Miyao,H., Ohkubo,K. and Suenobu,T. (2005) Electron-transfer oxidation properties of DNA bases and DNA oligomers. *J. Phys. Chem. A*, **109**, 3285–3294.